Environmental Interaction With Continuum Robots Exploiting Impact

Michael B. Wooten and Ian D. Walker

***Abstract*—Continuum robots offer unique potential benefits for environmental exploration, notably in using their maneuverability to navigate congested environments. However, significant challenges remain in environmental sensing using continuum structures, within which space for local sensing is often extremely limited. In this paper, we discuss the use of novel impulsive interaction using continuum robots to sense their environment. We introduce an impact model-based tapping approach with continuum robots which does not require the addition of specialized sensors, and demonstrate its utility in hardware. We contrast the impact model method to two alternative approaches to contact detection, "Finding Lost Wrenches" and the norm of the tendon length velocities. The methods are compared empirically on two different types of continuum robot hardware, a tendon actuated "Tendril" and the pneumatically actuated "OctArm". The results identify relative strengths and weaknesses of the approaches. The statics-based "Finding Lost Wrenches" approach failed when the manipulators were in motion, and the length velocity norm method suffered in cases of reduced sensor resolution. The impact model approach is shown to include information not accessible to the other approaches.**

***Index Terms*—Continuum robotics, biologically-inspired robots, dynamic impact, environmental interaction, contact modeling.**

I. Introduction

CONTINUUM robots have a continuous backbone as their structure with the ability to bend at any point along it [1]–[3]. Being compliant along the entire length allows for operation in extremely congested and a-priori unknown environments. Continuum robots have been successfully developed for use in many medical applications, e.g., endoscopic procedures, that require the manipulator to negotiate the complex and congested environment inside the human body [4]. In the human body, contact with the environment is inherent but often slowly varying as the robot is guided through tubular body structures. Researchers have investigated various approaches to sense and measure such contact. Numerous approaches have been developed to detect contact using kinematics or the intrinsic force sensing capabilities of continuum robots [5]–[9]. However, much of the existing research has concentrated on quasi-static conditions, and/or been motivated by the desire to minimize contact where possible [10]. Additionally, with medical procedures typically guided by the (a-priori known) topology of the human anatomy, the identification of a-priori unknown features has not been a priority.

Sensing of environmental features in a-priori unknown environments remains an open problem for continuum robots. Note that investigation and exploration of congested, hard-to-reach spaces has long been one of the main motivations for continuum robots. Long, thin "tendril" continuum robots have been proposed for exploration of various congested environments, including animal habitats and equipment racks on board the International Space Station [11], [12]. These structures have been demonstrated to be physically capable of negotiating tight and congested paths. However, environmental interaction and sensing of these types of environments remains an under-explored topic. In [13], obstacles are recognized as helpful in guiding the growth of vine-inspired continuum structures. However, such features need to be identified.

In this paper, we exploit impulsive interaction between continuum robots and their environment via active tapping, i.e., purposefully activating the robot to contact the environment with non-zero relative acceleration (i.e., not quasi-static contact), and inferring information about the environment from the result. Note that tapping is a technique that humans use for investigating their environments [14], [15]. Active tapping has been used as a strategy in numerous aspects of health, science, and engineering [16]–[18]. Information potentially available from such active physical interaction cannot be obtained using passive non-contact sensing, e.g., a tip camera. Note that tapping is inherently a dynamic process, involving the dynamics of impact.

While the dynamics of robotic systems (particularly rigid-link robot systems) moving in open space has been well-investigated, models involving robot impact with the environment is a much less explored topic. While there has, for example, been fairly extensive work in modeling impacts inherent in legged robot locomotion [19], [20], such efforts have concentrated on rigid-body impact. The dynamics of impact is indeed well-understood for collisions involving systems of rigid bodies [21], [22]. These general models for systems of rigid bodies have correspondingly been adapted to rigid-link robot arms contacting rigid elements of their environment [23]–[25].

The dynamics of environmental impact involving compliant, soft-bodied robots remains less well-understood, however. Impact-based grasping and manipulation with a continuum "tendril" robot was reported in [26]. However, that robot was not

Manuscript received 24 February 2022; accepted 28 June 2022. Date of publication 20 July 2022; date of current version 2 August 2022. This letter was recommended for publication by Associate Editor Y. Sun and Editor H. Liu upon evaluation of the reviewers' comments. This work was supported by U.S. National_Science_Foundation under NRI Grant 1924721. *(Corresponding author: Michael B. Wooten.)*

The authors are with the Department of Electrical and Computer Engineering, Clemson University, Clemson, SC 29634 USA (e-mail: mbwoote@g.clemson.edu; iwalker@clemson.edu).

Digital Object Identifier 10.1109/LRA.2022.3192771

2377-3766 © 2022 IEEE. Personal use is permitted, but republication/redistribution requires IEEE permission.
See https://www.ieee.org/publications/rights/index.html for more information.

Authorized licensed use limited to: CLEMSON UNIVERSITY. Downloaded on August 03,2022 at 01:11:10 UTC from IEEE Xplore. Restrictions apply.

operated using a model, instead guided heuristically to make contact, with the contact planned based on intuition. The first work explicitly considering environmental contact dynamics for continuum robotics appears to be [27], in which a physics engine was used to simulate the contact of a continuum robot section with a wall. A statics-based approach to contact detection for soft robots was recently introduced in [28], in which a Fixed Centrode Deviation (FCD) approach was employed to detect the contact position. Models for continuum robot impact dynamics are however currently lacking.

In this paper we introduce a new approach to environmental sensing for continuum robots via tapping, based on exploiting impact dynamics. We introduce a new approach to modeling impacts for continuum robots, and explore its utility in comparison with two alternative approaches. The models are described in Section II, with the new impact model introduced in Section II-C. We discuss the implementation of the models on two alternative types of continuum robot, and discuss the results obtained, in Sections III and IV, respectively. Conclusions are presented in Section V.

II. Continuum Robot Dynamics, Contact, and Impact Models

Tapping is a form of active touch [29], and to take advantage of it, algorithms need to be matched to the available sensors. Given the limitations on physical space, weight, and sensor input ports on typical continuum robots, assumptions of the availability of specialized exteroceptive sensors (force transducers, RGBD sensors, etc.) are questionable in practise. Therefore, in this work, we assume only real-time availability of proprioceptive configuration space (backbone shape) and, possibly, input effort (tendon tension or pressure) sensing. These sensing modalities are available on the robots used for empirical validation in this work (see Section III). The methods discussed in this section for contact/impact modeling below thus assume only configuration space (position) and, in one case, actuator effort information.

A. Underlying Continuum Robot Dynamic Model

We assume closed form dynamics for continuum manipulators with structure [30]:

$$\tau = [D(Q)]\ddot{Q} + [C(Q,\dot{Q})]\dot{Q} + [B(Q)] + [E(Q)] + g(Q) + [J_{xQ}(Q)]^T F \tag{1}$$

where τ is the actuator effort (tendon tensions, artificial muscle air pressures, etc.), and F represents the external force acting at the location of contact/impact with the environment. Q represents the configuration space, herein expressed in terms of s, k, ϕ, where these terms represent manipulator arc length, curvature, and bending angle plane respectively. $J_{xQ}(q)$ is the Jacobian relating configuration space to contact coordinates. $C(Q,\dot{Q})$ represents nonlinear effects, $B(Q)$ and $E(Q)$ the effects of backbone bending and extension (where applicable), respectively, and $g(Q)$ are the effects due to gravity, all as seen by the configuration space sensors.

B. Static Contact Modeling

1) Finding Lost Wrenches (LW): An innovative method for contact sensing for tendon-driven robots, termed "finding lost wrenches" and referenced herein as LW, was developed in [31], and its implementation is summarized by (2). This method is based on static balancing when no external forces are acting on the robot. In the notation used here, the approach becomes the following:

$$||J_{QL}^T(\tau') - \nabla E_{BEg}(Q)|| > \mathcal{E} \tag{2}$$

where the Jacobian J_{QL} maps configuration space velocities $\dot{Q}$ to tendon length velocities $\dot{L}$, $J_{QL}^T(\tau') = \tau$ in (1), τ' represents tendon tension feedback, and $\nabla E_{BEg}(Q)$ represents the gradient of the total elastic energy of the robot, modeling the internal forces from material properties [32], and modified herein to include the addition of gravitational forces [33]. The Jacobian relating tendon lengths to (s,k,ϕ) configuration space was derived from the analysis presented in [34]. Equation (3) presents this Jacobian for the tendril robot. The first column is zero because the tendril used herein was non-extensible. Equation (4) was used to calculate the gravitational effects on tendon tensions caused by configuration, representing $\nabla E_{BEg}(Q)$.

$$J_{QL} = \begin{bmatrix} 0 & -sR\cos\phi & sRk\sin\phi \\ 0 & -sR\cos\frac{2\pi}{3}-\phi & sRk\sin\frac{2\pi}{3}-\phi \\ 0 & -sR\cos\frac{4\pi}{3}-\phi & sRk\sin\frac{4\pi}{3}-\phi \end{bmatrix} \tag{3}$$

$$g_i(Q) = \frac{mg}{3\theta^2}\left(\cos\theta - \frac{1}{2}\cos 2\theta - \frac{1}{2}\right) - \frac{2\cos\alpha_i}{3R_a}\left\{\frac{EI\theta}{s} + \frac{mgs}{\theta^2}\left[\frac{1}{\theta}(\cos 2\theta - 2\cos\theta + 1) + (\sin 2\theta - \sin\theta)\right]\right\}, i = 1,2,3 \tag{4}$$

Nominally, in static non-contact operation, the output of the left hand side of (2) is zero, but external contact will increase the value. Contact is assumed when the output value increases over a pre-set threshold limit, $\mathcal{E}$, when it is inferred contact was made [31]. In this paper, we explore the potential of this measure to detect impulsive tapping, implementing it on a single section tendril robot (see Section III).

2) Finding Lost Pressures (LP): In this work, a modification of LW, "finding lost pressures" (referenced herein as LP), is introduced for use on the OctArm pneumatically actuated continuum robot system, due to the Octarm not having the tension sensing capabilities for which LW was developed. This new method was developed as an analog to the tension version, when we noticed that the disturbances in the pressure signals for the OctArm during contact events behaved similarly to tension signals during tendril experiments. This method simply replaces the τ' and $\nabla E_{BEg}(Q)$ in (2) with the measured pressure per muscle and subtracting the pressure target at that time, respectively. The OctArm manipulator was extensible, so its Jacobian includes a non-zero first column, which is presented in (5). Results from implementation of LP on the OctArm are reported and discussed

Authorized licensed use limited to: CLEMSON UNIVERSITY. Downloaded on August 03,2022 at 01:11:10 UTC from IEEE Xplore. Restrictions apply.

in Section III.

$$J_{QL} = \begin{bmatrix} 1 - Rk\cos\phi & -sR\cos\phi & sRk\sin\phi \\ 1 - Rk\cos\frac{2\pi}{3} - \phi & -sR\cos\frac{2\pi}{3} - \phi & sRk\sin\frac{2\pi}{3} - \phi \\ 1 - Rk\cos\frac{4\pi}{3} - \phi & -sR\cos\frac{4\pi}{3} - \phi & sRk\sin\frac{4\pi}{3} - \phi \end{bmatrix} \tag{5}$$

C. Models for Impact

1) Length Velocity Norm (LVN): Perhaps the simplest approach to measure contact using only position sensors is to use the length velocity norm. Given that each robotic system evaluated herein has tendon length sensing capabilities using string encoders that are parallel to the actuating tendons, tracking the rate of change in each tendon's length offers a relatively simple method for contact detection. Taking the 2-norm of the three length velocities in a single section results in a computationally simple non-negative measure with which to apply threshold sensing (6), the output of which will deviate from zero, when impulsive contact occurs. Note that the measure inherently also reflects velocity changes on normal operation. However, as we demonstrate in Section III, the above measure proves to be a fairly effective impact detector, in certain circumstances.

$$LVN = \sqrt{\left(\frac{\Delta L_1}{\Delta t}\right)^2 + \left(\frac{\Delta L_2}{\Delta t}\right)^2 + \left(\frac{\Delta L_3}{\Delta t}\right)^2} \tag{6}$$

2) Dynamic Impact Model (DIM): Next, we generalize a dynamic impact model (DIM) developed previously [23] for rigid-link manipulators to the case of continuum robot impact. That model assumes that the impact occurs in a small amount of time Δt, and that the bodies in contact do not deform significantly. Making the idealization, $\Delta t \to 0$ we define the (impulse) force at the contact point resulting from the impact as:

$$\hat{F} = \lim_{\Delta t \to 0} \int_t^{t+\Delta t} F(\tau) d\tau \tag{7}$$

Integrating (1) over $(t, t + \Delta t)$, taking $\Delta t \to 0$, and noting that in this infinitesimally small time of impact all velocities and angular velocities remain finite and there is no change in positions or orientations, we obtain the following relationship between $\hat{F}$ and changes in configuration velocities $\Delta\dot{Q} = (\dot{Q}(t + \Delta t) - \dot{Q}(t))$ [23]:

$$\Delta\dot{Q} = [D(Q)]^{-1}[J_{xQ}(Q)]^T\hat{F} \tag{8}$$

where as in (1), $[D(Q)]$ is the inertia matrix of the robot arm (assumed to be composed of serially connected rigid bodies in [23], but instead the corresponding matrix for continuum robots herein), and $[J_{xQ}(Q)]$ is the continuum robot Jacobian in (1) relating configuration to contact space variables. Inverting this relationship to compute $[J_{xQ}^{-T}(Q)][D(Q)]\Delta\dot{Q}$, we can estimate $\hat{F}$, and hence the magnitude and direction of impulse forces generated by tapping.

Note that the inversion of (8) to calculate $\hat{F}$ requires only the use of configuration space sensors. The implementation of (8) using continuum robot dynamics (1) in Section III of this paper is the first application of dynamic impact models to continuum robots, to the best of our knowledge.

The tendril robot is modeled as a point mass, with a mass of m_1, affixed to the tip of single section of a non-compressible elastic rod. Any bending in the rod is also assumed to be of constant curvature, or uniform bending curvature at any point along the backbone. The position of the point mass is given by (9). Solving for the velocities of the point mass results in (10) shown at the bottom of this page. From that definition, we can extract the Jacobian (J_xQ), presented in (11) shown at the bottom of this page.

Using (10), we define the kinetic energy of the system as $KE = \frac{1}{2}m_1\dot{\underline{x}}_1{}^T\dot{\underline{x}}_1$. The result of which can be expanded to extract the inertia matrix, presented in (12), shown at the bottom of this page. for the tendril robot in the dynamic impact model.

$$\underline{x}_1 = \begin{bmatrix} \frac{1}{k}\{\cos\phi(1 - \cos(sk))\} \\ \frac{1}{k}\{\sin\phi(1 - \cos(sk))\} \\ \frac{1}{k}\{\sin(sk))\} \end{bmatrix} \tag{9}$$

In the following, we compare and contrast the implementation of the three approaches discussed in this section: dynamic

$$\dot{\underline{x}}_1 = \begin{bmatrix} \cos\phi\sin(sk)\dot{s} + \frac{[(sk)\cos\phi\sin(sk) - (1-\cos(sk))\cos\phi]}{k^2}\dot{k} - \frac{[(sk)\cos\phi\sin(sk) - (1-\cos(sk))\cos\phi]}{k^2}\dot{\phi} \\ \sin\phi\sin(sk)\dot{s} + \frac{(sk)\sin\phi\sin(sk) - (1-\cos(sk))\sin\phi}{k^2}\dot{k} + \frac{(1-\cos(sk))\cos\phi}{k}\dot{\phi} \\ \cos(sk)\dot{s} + \frac{(sk)\cos(sk) - \sin(sk)}{k^2}\dot{k} \end{bmatrix} \tag{10}$$

$$J_{xQ} = \begin{bmatrix} \cos\phi\sin(sk) & \frac{[(sk)\cos\phi\sin(sk) - (1-\cos(sk))\cos\phi]}{k^2} & -\frac{(1-\cos(sk))\sin\phi}{k} \\ \sin\phi\sin(sk) & \frac{(sk)\sin\phi\sin(sk) - (1-\cos(sk))\sin\phi}{k^2} & \frac{(1-\cos(sk))\cos\phi}{k} \\ \cos(sk) & \frac{(sk)\cos(sk) - \sin(sk)}{k^2} & 0 \end{bmatrix} \tag{11}$$

$$D(Q) = \begin{bmatrix} m_1 & m_1\left[(\frac{s}{k})\sin^2(sk) - \left(\frac{\sin(sk)(1-\cos(sk))}{k^2}\right)\right] & 0 \\ m_1\left[(\frac{s}{k})\sin^2(sk) - \left(\frac{\sin(sk)(1-\cos(sk))}{k^2}\right)\right] & m_1(*) & 0 \\ 0 & 0 & m_1\left[\frac{1-\cos(sk)}{k^2}\right]^2 \end{bmatrix} \tag{12}$$

$$\text{where } (*) = \left[\left((\frac{s}{k})^2\sin^2(sk)\right) + \left(\frac{1-\cos(sk)}{k^2}\right)^2 - \left[\left(\frac{s}{k^3}\right)(\sin(sk)(1-\cos(sk)))\right]\right]$$

Authorized licensed use limited to: CLEMSON UNIVERSITY. Downloaded on August 03,2022 at 01:11:10 UTC from IEEE Xplore. Restrictions apply.

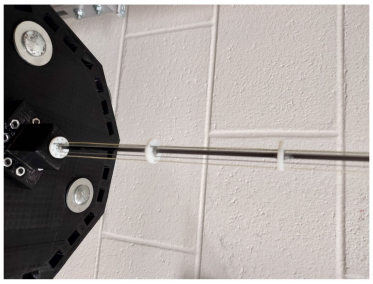

Fig. 1. Image of tendril robot's base section where it interfaces with the actuator package.

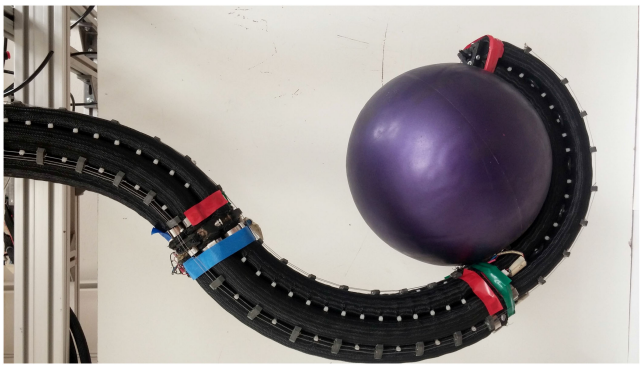

Fig. 2. OctArm continuum manipulator. String encoder sensors can be seen on outer surface.

impact DIM; length velocity norm LVN; and finding lost effort (wrenches (FW) for tendon actuation/pressures (FP) for pneumatic actuation).

III. Implementation of Impact Models

Experiments were conducted in a lab setting to assess the capabilities and limitations of each of the approaches discussed above. The methods were implemented on two different types of continuum robot hardware, described in the following subsection.

A. Tendril and OctArm Hardware

The methods and models discussed herein were implemented on two separate robotic systems. The first system used in this work is a tendril continuum robot (Fig. 1); a tendon driven, long thin continuum robot [11], [12], [35]. These robots are typically comprised of multiple sections, each actuated using three tendons; each of which has tension sensing (model: FC2231-0000-0050-L, Measurement Specialties^{TM}) and a motor encoder to track tendon movement. In this work, the system has been further modified by the addition of string encoders for each tendon, similar to their implementation in the OctArm, discussed below. These string encoders give real time tendon length feedback.

The second robot was the OctArm: a three section pneumatic continuum robot [36], shown in Fig. 2. Each section is made up of three, or three sets of two, McKibben muscles driven by pressurized air. Each muscle is connected to a pressure regulator and a string encoder [37]. During operation, the OctArm manipulator is actuated by setting pressure values for regulators connected to each muscle. Sensor feedback for the system consists of the raw pressures, which the regulators attempt to keep at the given pressure settings, and a string encoder per muscle that gives muscle length feedback. Three lengths tracked per section using the string encoders provide real-time sensing of configuration.

TABLE I
Physical Parameters Used in Implementation

Device	Mass (g)	Length (m)	Radius (m)	E (Nm^{-2})	I (m^4)
Tendril	12	0.931	0.005	94.52	1.67E-12
OctArm	500	Variable	0.033	N/A	N/A

The physical parameters of each robotic system are detailed in Table I. These values variables are used in each method as described in the previous section.

B. Experimental Procedures

Experiments with both robotic systems were conducted, with both initial static configurations, and dynamic robot movement at the time environmental contact was made. In the initial static cases, used mostly to validate the implementation of the measures of Section II, each of the two continuum manipulators was held static in various configurations. While in the static state, contact was made by a human using a stick with a flat plate at its end, varying both magnitude and direction of the applied forces. The flat plate used to make contact was 4 cm wide and 10 cm long and made contact with each robotic manipulator as near the tip as possible.

During dynamic tests, the procedure was similar with the notable exception of each manipulator undergoing constant motion, with configuration changing throughout the experiment. Initially the magnitude was not quantitatively measured and relied on the operator applying their own ability to judge forces applied to the manipulators throughout the experiments. In either the static or dynamic case, the manipulator was struck between one and four times on average. During each experiment, all sensor data for each system was recorded and processed offline in MATLAB.

Subsequent experiments were conducted with the tendril robot inserted into a box. The tendril was deployed to move in a roughly circular trajectory of the tip, reminiscent of circumnutation patterns used by thin plants such as vines to explore their environments [35]. On contact with the environment, the robot was commanded to tap (iteratively reverse direction and then reverse back to make impulsive contact). The goal of the experiment was to identify the locations of environmental obstacles, and identify significant features. The results of the experiments are reported and discussed in the following section.

IV. Results and Discussion

The results of the experiments demonstrate the relative capabilities of the contact detection methods introduced in Section II. The set of graphs that make up Fig. 3 are the results from a typical experiment using the tendril, in which the manipulator is held static at a chosen configuration. In this specific data set,

Authorized licensed use limited to: CLEMSON UNIVERSITY. Downloaded on August 03,2022 at 01:11:10 UTC from IEEE Xplore. Restrictions apply.

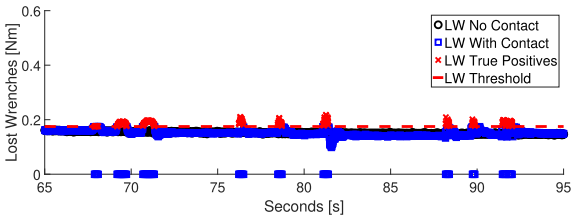

(a) Finding Lost Wrenches

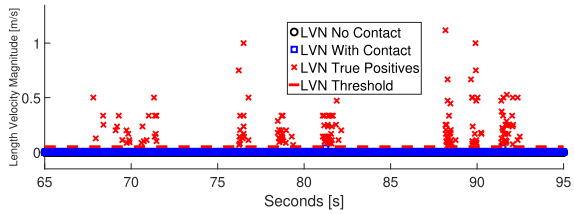

(b) Length Velocity Norm

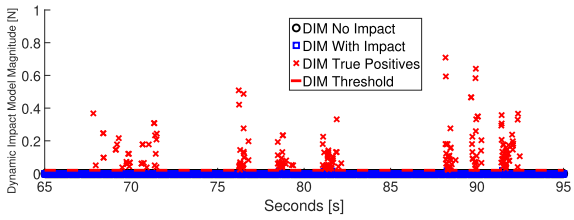

(c) Dynamic Impact

Fig. 3. Tendril impact model outputs when manipulator is static.

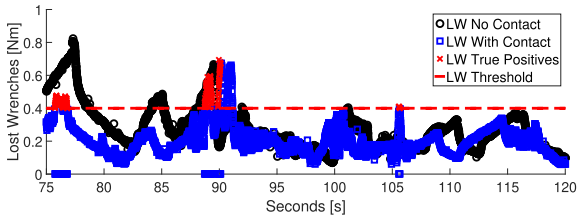

(a) Finding Lost Wrenches

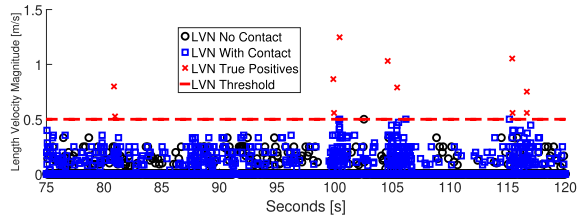

(b) Length Velocity Norm

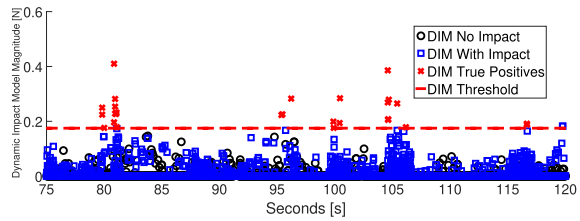

(c) Dynamic Impact

Fig. 4. Tendril impact model outputs when manipulator is in motion.

TABLE II
PERCENTAGE OF TOTAL PROCESSING TIME FOR EACH METHOD PRESENTED ABOVE

Experiment Processing	Total Run Time (s)	LW or LP Run Time (%)	LVN Run Time (%)	DIM Run Time (%)
Static Tendril	4.7669 s	4.73%	3.16%	9.60%
Dynamic Tendril	0.6927 s	18.4%	10.8%	34.5%
Static Octarm	0.1191 s	20.8%	11.8%	41.1%
Dynamic Octarm	0.2451 s	13.5%	20.5%	37.5%

the contact forces were generated manually and the magnitude of force applied was increased over time. The graphs show the output of each method discussed in Section II, where Fig. 3(a) is the result of finding lost wrenches, Fig. 3(b) is the length velocity norm, and Fig. 3(c) is the dynamic impact model output. In the subsequent series of figures, each set of graphs will appear in the same order. Accompanied by each data set is a baseline (labelled as baseline and in black) in which no contact was made for each individual experiment, so every graph is contrasted by a data set in which no contact occurred. When processing the experimental data, if a model's output signal value increased over a certain threshold during a manually verified time in which contact was occurring, then the datum was considered a true positive. In the following graphs, this distinction is represented by a change of color and marker type; blue squares are the output data of the given model and a red "x" indicates a true positive. Table II presents the percentage of total processing time taken to compute the output of each method for each of the experiments presented below. The DIM is generally the most computationally expensive with LVN the least computationally expensive. However, this difference is only a factor of between 2 and 4.

A. *Static Tendril*

Fig. 3 showcases an experiment where a single section of the tendril robot was held static at various configurations during instances of contact. Output for our implementation of finding lost wrenches is heavily affected, even in the baseline data, by changes in configuration throughout the experiment, rendering it ineffective. This was consistent across experiments. Hence, from now on, we concentrate on the length velocity norm and impact model. When using the length velocities in the tendril robot, we observed it to be less effective than when used in the Octarm. This decline in functionality was attributed to the diameter difference in the two devices and the resulting loss of resolution of the string encoders in the tendril for tracking changes. The dynamic impact model however, though the resolution is lower, still produces impulses at time of contact. The threshold values for this set are 0.175 Nm, 0.05 m/s, and 0.02 N for LW, LVN, and DIM, respectively.

B. *Dynamic Tendril*

Fig. 4 depicts the results of an experiment where the tendril robot was in motion throughout the experiment, while contact was made by the user and marked when contacts were to be made. The "Finding Lost Wrenches" method, as was the case

Authorized licensed use limited to: CLEMSON UNIVERSITY. Downloaded on August 03,2022 at 01:11:10 UTC from IEEE Xplore. Restrictions apply.

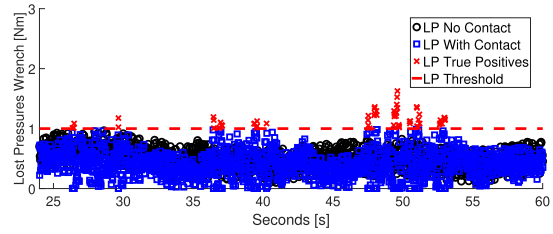

(a) Finding lost pressures

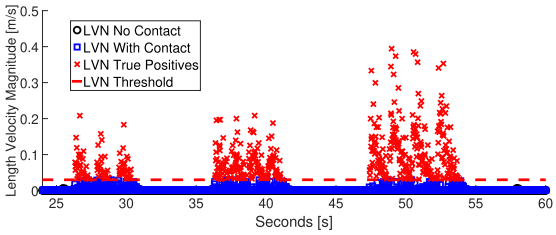

(b) Length Velocity Norm

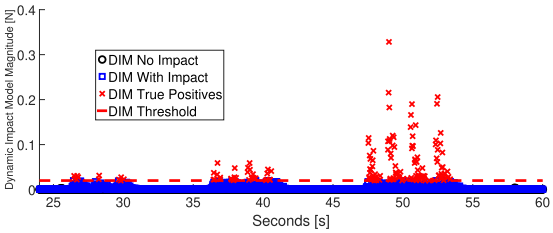

(c) Dynamic Impact

Fig. 5. OctArm manipulator in static configuration with contact forces increasing in magnitude over time.

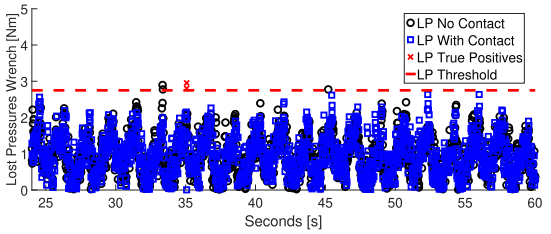

(a) Finding Lost Pressures

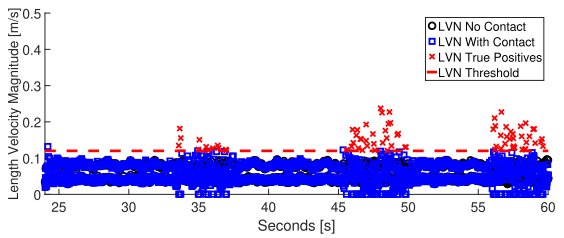

(b) Length Velocity Norm

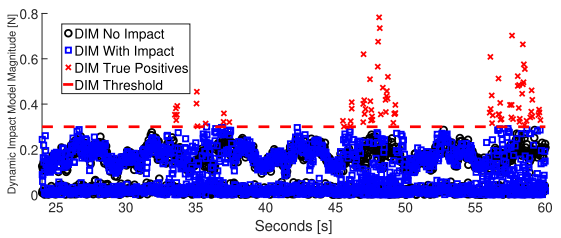

(c) Dynamic Impact

Fig. 6. Model outputs of data from Octarm manipulator being contacted while in motion.

with the Octarm, is incapable of adequately sensing the contact via a threshold, because it relies on the condition that the robot is static. When in motion, the algorithm output changes over time as the internal forces change. Length velocities are still shown to be useful, but the movement increases noise in the signal making it more difficult to distinguish from the baseline data, which would result in more false positives during operation. In the same experimental data, the dynamic impact model is shown in Fig. 4(c) to more accurately detect these impulse forces than the other methods presented. The threshold values for this set are $0.4Nm$, 0.5 m/s, and 0.175 N for LW, LVN, and DIM, respectively.

C. Static OctArm

Fig. 5(a) indicates that when the robot is static (i.e., impact is initiated by the environment) the "finding lost pressures" (LP) algorithm could successfully detect the contact at most contact magnitudes. If we considered threshold values of $\mathcal{E} = 1Nm$, 0.03 m/s, and 0.02 N to assume contact for the LP, LVN, and DIM methods, respectively. The LVN [Fig. 5(b)] and DIM [Fig. 5(c)] methods in the static case show even more distinct differences from the baseline, indicating a higher sensitivity to impacts compared to the pressure based method derived from (2). The threshold values are represented in the figures below as horizontal red dotted lines.

D. Dynamic OctArm

Fig. 6 shows the graphs of the three model outputs in a typical example of the OctArm manipulator being in active motion. Under this operational condition, it can be seen that the pressure based model has a significant reduction in signal clarity - and therefore performance. This reduces the method to the point of being unusable when the static condition cannot be assumed, as instances of contact become difficult to differentiate from signal noise (which also appears in the baseline data). However, in each of the other two impact models, contact instances remain easily differentiated both from the baseline data set and during normal, non-contact operation. The threshold values for this set are 2.75 Nm, 0.12 m/s, and 0.3 N for LP, LVN, and DIM, respectively.

E. Further Experiments

As an evaluation of the ability of the methods to support continuum robot tapping, the tendril robot was deployed inside a box. The goal of this experiment (the setup similar to one performed in [9]) was for the robot to interact with the environment via tapping, and identify key features of the box. Fig. 7 shows 0.215 m of the tendril inserted into the box, which had an open top and measured 0.4 m $\times$ 0.385 m in the horizontal plane. The tendril section was bent (from zero curvature) within the box, in a series of planes varying in rotation about the vertical

Authorized licensed use limited to: CLEMSON UNIVERSITY. Downloaded on August 03,2022 at 01:11:10 UTC from IEEE Xplore. Restrictions apply.

(a) Tendril straining against barrier.

(b) Tendril suddenly shifting obstacle.

Fig. 7. Image of tendril robot inserted into box.

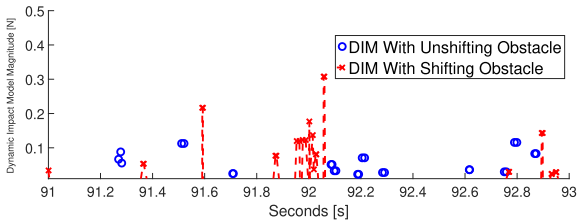

Fig. 8. Box experiment. Plot showing spike at 92 s when box side suddenly opens under tapping and interacts with tendril.

(backbone initial tangent, this rotation defining azimuth here), with two taps performed on contact with the box at each plane, over a pre-selected set of azimuth angles.

In the box experiments, the flap comprising one side of the box was initially held closed by a piece of tape, to secure the box so it remained closed throughout the experiment, in a way that active tapping on that surface would cause the flap to open. This was done to explore more complex dynamic environmental interactions using tapping which modify the environment and potentially generate new information about it (in this case revealing a new and previously unobservable way to exit the box), in a way not possible with non-contact operation.

Representative results from the box experiments are illustrated in Fig. 8. We recognize that non-contact sensors, e.g., tip cameras, represent an alternative (and higher fidelity) way to sense the internal geometry of a box, at the cost of incorporation of such additional sensors. This experiment demonstrated additional capabilities of the dynamic impact approach. In Fig. 8, the output of the impact model is displayed, for the case where the box was less securely taped, and tapping opened the flap, bouncing it against the tendril. It can be seen from the data that as the box flap interacts dynamically with the tendril, and this sudden shift in an obstacle occurs, the DIM method is shown capable of clearly seeing the sudden change in configuration velocities; as large output values of DIM occur. This dynamic phenomenon was not reliably observed in the length velocity norm output. This demonstrates the ability of the dynamics-based approach to infer structural/physical properties of the environment that would not have been sensed with non-contact operations such as a tip camera.

To validate the DIM model's accuracy we performed a series of experiments to measure the impulsive forces acting on the tip of the tendril robot. We added a 3D printed structure to a compression load cell that was used to tap the tendril robot during operation. A simple calibration, using known weights, was performed to relate sensor voltage to force in Newtons. Using timestamp matching the impulses generated by both the DIM method and the load cell forces were lined up and compared for accuracy. Taking a representative sample of such overlapping impulses, the forces were shown to range from 0.1791 N to 0.7701 N, with a mean of 0.3264 N. The average error between these readings and the corresponding modeled impulses was found to be 0.1449 N.

F. Discussion

The results of these experiments illustrate the relative capabilities of the three methods. The "finding lost wrenches" method data is noisy, and as noted above, not preferred in the impulsive interaction context. This is not surprising, as that approach is based on statics, and the contacts considered in the experiments are impulsive, i.e., dynamic, in nature. The dynamic impact method performs better than the velocity norm in all cases. The velocity norm method does have the advantage of being inherently computationally less intensive, but the impact model based approach gives higher fidelity results, proving a better differentiator of contact in general, and being the only method to reliably reflect the dynamic opening of the side of the box.

V. Conclusion

We present a novel approach to continuum robot environmental interaction, based on tapping. The approach does not require the addition of specialized sensors to implement, and is implementable in real time. We introduce a model of impact dynamics for continuum robots, and use it to detect the effects of impulsive, i.e., tapping-based, environmental interaction. We compare the impact model-based approach with two other contact models: configuration space velocity differences and force balancing based on statics. The three methods are each implemented on two different types of continuum robot: a tendon-actuated tendril and a pneumatically actuated manipulator.

The results demonstrate that impulsive tapping can be an effective technique for identification of some environmental features. The dynamic impact model-based approach is shown to provide useful information about the environment, i.e., properties only observable via physical interaction, not accessible from the statics or velocity based methods.

Acknowledgment

The authors would like to thank Chase Frazelle for his help in performing the experiments with the Octarm manipulator.

References

[1] D. Trivedi, C. D. Rahn, W. M. Kier, and I. D. Walker, "Soft robotics: Biological inspiration, state of the art, and future research," *Appl. Bionics Biomech.*, vol. 5, no. 3, pp. 99–117, 2008.

[2] I. D. Walker, H. Choset, and G. Chirikjian, "Snake-like and continuum robots," in *Springer Handbook of Robotics*, 2nd ed. Berlin, Germany: Springer, 2016, ch. 20, pp. 481–498.

[3] R. J. Webster and B. A. Jones, "Design and kinematic modeling of constant curvature continuum robots: A review," *Int. J. Robot. Res.*, vol. 29, no. 13, pp. 1661–1683, 2010.

Authorized licensed use limited to: CLEMSON UNIVERSITY. Downloaded on August 03,2022 at 01:11:10 UTC from IEEE Xplore. Restrictions apply.

[4] J. Burgner-Kahrs, D. C. Rucker, and H. Choset, "Continuum robots for medical applications: A survey," *IEEE Trans. Robot.*, vol. 31, no. 6, pp. 1261–1280, Dec. 2015.
[5] M. Mahvash and P. E. Dupont, "Stiffness control of a continuum manipulator in contact with a soft environment," in *Proc. IEEE/RSJ Int. Conf. Intell. Robots Syst.*, 2010, pp. 863–870.
[6] K. Oliver-Butler, J. Till, and D. C. Rucker, "Continuum robot stiffness under external loads and prescribed tendon displacements," *IEEE Trans. Robot.*, vol. 35, no. 2, pp. 403–419, Apr. 2019.
[7] R. Roy, L. Wang, and N. Simaan, "Investigation of effects of dynamics on intrinsic wrench sensing in continuum robots," in *Proc. IEEE Int. Conf. Robot. Automat.*, 2016, pp. 2052–2059.
[8] D. C. Rucker and R. J. Webster, "Deflection-based force sensing for continuum robots: A probabilistic approach," in *Proc. IEEE/RSJ Int. Conf. Intell. Robots Syst.*, 2011, pp. 3764–3769.
[9] S. Tully, A. Bajo, G. Kantor, H. Choset, and N. Simaan, "Constrained filtering with contact detection for the localization and registration of continuum robots in flexible environments," in *Proc. IEEE Int. Conf. Robot. Automat.*, 2012, pp. 3388–3394.
[10] Z. Zhang, J. Dequidt, J. Back, H. Liu, and C. Duriez, "Motion control of cable-driven continuum catheter robot through contacts," *IEEE Robot. Automat. Lett.*, vol. 4, no. 2, pp. 1852–1859, Apr. 2019.
[11] M. Wooten and I. Walker, "Vine-inspired continuum tendril robots and circumnutations," *Robotics*, vol. 7, no. 3, 2018, Art. no. 58.
[12] M. Wooten, C. Frazelle, I. D. Walker, A. Kapadia, and J. H. Lee, "Exploration and inspection with vine-inspired continuum robots," in *Proc. IEEE Int. Conf. Robot. Automat.*, 2018, pp. 5526–5533.
[13] J. D. Greer, L. H. Blumenschein, A. M. Okamura, and E. W. Hawkes, "Obstacle-aided navigation of a soft growing robot," in *Proc. IEEE Int. Conf. Robot. Automat.*, 2018, pp. 4165–4172.
[14] K. Higashi, S. Okamoto, and Y. Yamada, "What is the hardness perceived by tapping?," in *Proc. 10th Int. Conf. Haptics: Perception, Devices, Control, Appl.–Part I*, 2016, vol. 9774, pp. 3–12.
[15] B. N. Schenkman and G. Jansson, "The detection and localization of objects by the blind with the aid of long-cane tapping sounds," *Hum. Factors*, vol. 28, no. 5, pp. 607–618, 1986.
[16] D. Church, P. Stapleton, A. Yang, and F. Gallo, "Is tapping on acupuncture points an active ingredient in emotional freedom techniques? A systematic review and meta-analysis of comparative studies," *J. Nervous Ment. Dis.*, vol. 206, no. 10, pp. 783–793, 2018.
[17] P. K. Hansma et al., "Tapping mode atomic force microscopy in liquids," *Appl. Phys. Lett.*, vol. 64, no. 13, Art. no. 1738, 1994.
[18] Q. Kong, J. Zhu, S. Chun, M. Ho, and G. Song, "Tapping and listening: A new approach to bolt looseness monitoring," *Smart Mater. Struct.*, vol. 27, no. 7, 2018, Art no. 07LT02.
[19] A. W. Long, T. D. Murphey, and K. M. Lynch, "Optimal motion planning for a class of hybrid dynamical systems with impacts," in *Proc. IEEE Int. Conf. Robot. Automat.*, 2011, pp. 4220–4226.
[20] Y.-F. Zheng and H. Hemami, "Impact effects of biped contact with the environment," *IEEE Trans. Syst., Man, Cybern.*, vol. SMC-14, no. 3, pp. 437–443, May/Jun. 1894.
[21] Y. Wang and M. T. Mason, "Modeling impact dynamics for robotic operations," in *Proc. IEEE Int. Conf. Robot. Automat.*, 1987, pp. 678–685.
[22] J. Wittenburg, *Dynamics of Systems of Rigid Bodies*. Stuttgart, Germany: Teubner, 1977.
[23] I. D. Walker, "Impact configurations and measures for kinematically redundant and multiple armed robot systems," *IEEE Trans. Robot. Automat.*, vol. 10, no. 5, pp. 670–683, Oct. 1994.
[24] K. Yoshida, C. Mavroidis, and S. Dubowsky, "Impact dynamics of space long reach manipulators," in *Proc. IEEE Int. Conf. Robot. Automat.*, 1996, vol. 2, pp. 1909–1916.
[25] Y. F. Zheng and H. Hemami, "Mathematical modeling of a robot collision with its environment," *J. Robot. Syst.*, vol. 2, pp. 289–307, 1985.
[26] L. Cowan and I. D. Walker, "The importance of continuous and discrete elements in continuum robots," *Int. J. Adv. Robot. Syst.*, vol. 10, no. 3, 2013, Art. no. 165.
[27] J. Grey and I. S. Godage, "Realtime contact dynamics for continuum arms using physics engines," in *Proc. IEEE/RSJ Int. Conf. Intell. Robots Syst.*, 2019, Art. no. 3364.
[28] Y. Chen, L. Wang, K. Galloway, I. Godage, N. Simaan, and E. Barth, "Model-based kinematics and contact detection of soft robots," *Soft Robot.*, vol. 8, no. 3, pp. 298–309, 2021.
[29] R. A. Grant, P. M. Itskov, R. M. Towal, and T. J. Prescott, "Active touch sensing: Finger tips, whiskers, and antennae," *Front. Behav. Neurosci.*, vol. 8, 2014, Art. no. 50.
[30] E. Tatlicioglu, I. D. Walker, and D. M. Dawson, "New dynamic models for planar extensible continuum robot manipulators," in *Proc. IEEE/RSJ Int. Conf. Intell. Robot. Syst.*, 2007, pp. 1485–1490.
[31] A. Bajo and N. Simaan, "Finding lost wrenches: Using continuum robots for contact detection and estimation of contact location," in *Proc. IEEE Int. Conf. Robot. Automat.*, 2010, pp. 3666–3673.
[32] M. M. Dalvand, S. Nahavandi, and R. D. Howe, "An analytical loading model for *n*-tendon continuum robots," *IEEE Trans. Robot.*, vol. 34, no. 5, pp. 1215–1225, Oct. 2018.
[33] P. Sterckx and I. D. Walker, "Modeling and design optimization of robotic hoses for 3D printing of cement," in *Proc. ASME Int. Mech. Eng. Congr. Expo.*, 2020, pp. 1–6.
[34] B. A. Jones and I. D. Walker, "Kinematics for multi-section continuum robots," *IEEE Trans. Robot.*, vol. 22, no. 1, pp. 43–55, Feb. 2006.
[35] M. B. Wooten and I. D. Walker, "Circumnutation: From plants to robots," in *Proc. From Animals Animats:14th Int. Conf. Simul. Adaptive Behav.*, 2016, pp. 1–11.
[36] W. McMahan et al., "Field trials and testing of OCTARM continuum robots," in *Proc. IEEE Int. Conf. Robot. Automat.*, 2006, pp. 2336–2341.
[37] I. D. Walker et al., "Continuum robot arms inspired by cephalopods," in *Proc. SPIE Conf. Unmanned Ground Veh. Technol. VII*, 2005, pp. 303–314.

Authorized licensed use limited to: CLEMSON UNIVERSITY. Downloaded on August 03,2022 at 01:11:10 UTC from IEEE Xplore. Restrictions apply.